Korean J. Chem. Eng., 37(10), 1680-1689 (2020)
DOI: 10.1007/s11814-020-0573-7

pISSN: 0256-1115
eISSN: 1975-7220

Development of highly selective In_2O_3/ZrO_2 catalyst for hydrogenation of CO_2 to methanol: An insight into the catalyst preparation method

Munirah Md Zain*, Maedeh Mohammadi, Naoto Kamiuchi***, and Abdul Rahman Mohamed*,†**

*Low Carbon Economy (LCE) Research Group, School of Chemical Engineering, Universiti Sains Malaysia, 14300 Nibong Tebal, Pulau Pinang, Malaysia
**Faculty of Chemical Engineering, Babol Noshirvani University of Technology, 47148 Babol, Iran
***The Institute of Scientific and Industrial Research, Osaka University, 8-1 Mihogaoka, Ibaraki, Osaka 567-0047, Japan
(*Received 9 February 2020 • Revised 4 May 2020 • Accepted 11 May 2020*)

Abstract−This study explored the potential of In_2O_3/ZrO_2 catalyst for direct CO_2 hydrogenation to methanol. Despite the excellent properties proven by density functional theory (DFT) studies, the experimental works on this catalyst are still very limited. In this study, In_2O_3/ZrO_2 catalysts were synthesized via wetness impregnation (In_2O_3/ZrO_2(WI)), citric acid-based sol-gel method (In_2O_3/ZrO_2(SG)) and deposition-precipitation assisted by urea hydrolysis (In_2O_3/ZrO_2(UH)). Results indicated the impressive effect of preparation method on the catalytic activity where In_2O_3/ZrO_2(SG) presented superior catalytic performance, followed by In_2O_3/ZrO_2(UH) and In_2O_3/ZrO_2(WI), with the CO_2 conversion of 16.23%, methanol selectivity of 94.39% and STY of 0.95 $g_{methanol}/g_{cat}$·h. To unravel the structure-function relationship, several characterization techniques including XRD, HR-TEM, SEM-EDX, H_2-TPR, CO_2-TPD, N_2 adsorption-desorption isotherm and XPS were implemented to analyze the developed catalysts. The analyses indicated that the excellent performance of In_2O_3/ZrO_2 (SG) was due to its smaller crystallite size, strong metal-support interaction, high reducibility and high concentration of basic sites and oxygen vacancies on the catalyst surface. Time-on-stream stability test showed that In_2O_3/ZrO_2 (SG) catalyst could sustain its high activity and selectivity within 100 h, signifying the high potential of this catalyst for direct hydrogenation of CO_2 to methanol with minimum side reactions and deactivation.

Keywords: Heterogenous Catalyst, CO_2 Hydrogenation, Methanol Synthesis, Reducibility, Basic Sites, Oxygen Vacancies

INTRODUCTION

Carbon dioxide (CO_2) capture, utilization and storage (CCUS) has been proposed as a promising strategy to reduce the emission of CO_2 into the atmosphere. The captured CO_2 can be utilized as a C1 carbon feedstock for production of valuable fuels and chemicals such as methanol, which can be either utilized as a fuel or a starting material in chemical industries. Conventionally, for production of methanol, syngas is first produced via steam reforming of natural gas, then the produced syngas, which is a mixture of carbon monoxide (CO), hydrogen (H_2) and CO_2, is converted to methanol [1]. The direct synthesis of methanol via hydrogenation of CO_2 has gained tremendous attention due to the straightforward single step process compared to the conventional methanol production process. The hydrogenation of CO_2 to methanol occurs in the presence of H_2 (Eq. (1)). During the reaction, CO will also present as a by-product via the reverse-water-gas-shift (RWGS) side reaction (Eq. (2)). Naturally, RWGS reaction will be predominant at higher temperatures due to its endothermicity, and since the equilibrium CO_2 conversion increases at high temperatures a high rate of CO_2 conversion can be achieved [2]. The CO produced through the RWGS reaction can also be reduced to methanol according to Eq. (3). All these reactions occur simultaneously in the gas phase and are in chemical equilibrium [3]. However, since the reduction of carbon oxides to methanol (Eqs. (1) and (3)) is exothermic, therefore CO_2 hydrogenation to methanol must be conducted at lower temperatures to ensure higher selectivity of methanol as the desired product.

$$CO_2+3H_2\leftrightarrow CH_3OH+H_2O \qquad \Delta H_{298\,K}=-49.5\ kJ/mol \qquad (1)$$

$$CO_2+H_2\leftrightarrow CO+H_2O \qquad \Delta H_{298\,K}=+41\ kJ/mol \qquad (2)$$

$$CO+2H_2\leftrightarrow CH_3OH \qquad \Delta H_{298\,K}=-91\ kJ/mol \qquad (3)$$

Conventionally, only $Cu/ZnO/Al_2O_3$ catalyst has been used at industrial scale for commercial methanol production [4]. The use of high temperatures for Cu-based catalysts, however, results in the reduction of methanol selectivity, which means the RWGS reaction is encouraged and more undesired CO is produced. Thus, there is ongoing research to find a suitable catalyst that can overcome this deficiency and provide both high conversion efficiency and selectivity.

Indium oxide (In_2O_3) has a high potential as catalyst for CO_2 hydrogenation to methanol. Theoretical studies have shown that In_2O_3 can exhibit good catalytic performance, as it is expected to increase the methanol selectivity by supressing the RWGS reaction. Ye et al. [5], through a DFT study, showed that CO_2 hydrogenation to methanol follows a formate pathway and this can enhance the methanol selectivity. Previous experimental works have also proven that In-based catalysts are more active compared to other catalysts

†To whom correspondence should be addressed.
E-mail: chrahman@usm.my

for CO_2 hydrogenation to methanol. Sun et al. [6] discussed that use of In-based catalysts for CO_2 hydrogenation resulted in higher yield and formation rate compared to the conventional Cu-based catalyst at the same reaction condition. Stability also plays an important role in selection of suitable catalyst. Martin et al. [7] showed that In_2O_3 supported on zirconium oxide (ZrO_2) has higher stability and resistance towards catalyst deactivation compared to Cu-based catalyst. Despite the high potential of In-based catalysts for catalyzing the direct hydrogenation of CO_2 to methanol, so far very few investigations have been carried out on this catalyst. Especially, the effect of catalyst preparation method on its structural properties and catalytic activity is unrevealed.

With the aim of gaining some insights into the influence of catalyst synthesis method on its structure/performance, we investigated the preparation of In_2O_3 catalyst supported on ZrO_2, through different synthesis methods for CO_2 hydrogenation to methanol. Selection of ZrO_2 as the support was based on the results reported by Martin et al. [7], who supported In_2O_3 on various carriers and found that ZrO_2 demonstrated superior performance compared to other supports. Three different catalyst preparation methods, namely, wetness impregnation, citric acid-based sol-gel method, and deposition-precipitation assisted by urea hydrolysis, were used for catalyst development. The performance of the synthesized catalysts in the CO_2 hydrogenation reaction was evaluated. Moreover, several structural characterizations were carried out to justify the different catalytic performance of the catalysts in the reaction.

MATERIALS AND METHODS

1. Materials

Indium (III) nitrate hydrate 99.9% ($In(NO_3)_3 \cdot xH_2O$) and zirconium (IV) oxide 99.9% (ZrO_2) used as metal precursor and support, respectively, were obtained from Sigma Aldrich, USA. Urea (99%) for deposition-precipitation assisted by urea hydrolysis and citric acid (99%) for citric acid-based sol-gel synthesis methods were both obtained from Merck, Germany.

2. Catalyst Preparation

The catalyst used for CO_2 hydrogenation, In_2O_3 supported on ZrO_2 (In_2O_3/ZrO_2), was synthesized through three different methods: wetness impregnation (WI), citric acid-based sol-gel method (SG) and deposition-precipitation assisted by urea hydrolysis (UH). For WI method, 1.8 g of ZrO_2 was suspended in deionized water, then, 0.43 g $In(NO_3)_3 \cdot xH_2O$ was added to the solution to have 10 wt% In_2O_3 in the mixture. The suspension was stirred at 270 rpm for 5 h. The mixture was then dried in an oven at 105 °C for 24 h. The dried sample was then ground and calcined in air at 500 °C for 5 h. For SG method, the precursors with same amounts as those of WI methods were mixed in deionized water. Citric acid was then added to the solution; the mole ratio of citric acid to metal precursor was 3 : 1. The sample was stirred at 270 rpm until a gel-like product was formed. The drying and calcination procedures were the same as the WI method. With the UH method, urea was first dissolved in deionized water, then quantities of ZrO_2 and $In(NO_3)_3 \cdot xH_2O$, similar to other methods, were added to the mixture; the mole ratio of urea to metal precursor was 3 : 1. The sample was stirred at 270 rpm for 5 h, then it was dried and calcined as described. The catalysts prepared by WI, SG and UH methods were denoted as In_2O_3/ZrO_2(WI), In_2O_3/ZrO_2(SG) and In_2O_3/ZrO_2(UH), respectively.

3. Catalytic Activity Testing

The CO_2 hydrogenation reaction was conducted in a continuous flow fixed-bed vertical micro-reactor with inner diameter of 6 mm and length of 180 mm. In a typical experiment, 160 mg of the catalyst was packed between layers of glass beads and the reactant gases, H_2 and CO_2, with mole ratio of 3 : 1 were supplied into the reactor; the flows were regulated with mass flow controllers (Brooks Instrument). All experiments were conducted at 280 °C, 4 MPa and weight hourly space velocity (WHSV) of 15,000 mL/g_{cat}·h. Selection of such temperature and WHSV was based on the preliminary experiments carried out to find the conditions at which the highest catalytic performance could be achieved (Figs. S1 and S2). Samples were collected from the effluent every 20 min using automated gas sampling valve and analyzed by an on-line gas chromatograph (GC, Agilent 7890A) equipped with thermal conductivity detector (TCD). The products were separated by Hayesep T column. Helium was used as the carrier gas. The oven temperature was set at 150 °C. The concentration of unreacted feedstocks and products was determined using multiple point external standard method. The data collected within the time interval of 8 to 10 h of the operation, wherein steady-state condition was achieved, were used to calculate the average CO_2 conversion, selectivity, yield of product and space time yield (STY) according to the following equations:

$$\text{CO}_2 \text{ conversion, } X_{CO_2}(\%) = \frac{(nCO_{2,\,in} - nCO_{2,\,out})}{nCO_{2,\,in}} \tag{4}$$

$$\text{Selectivity, } S_i(\%) = \frac{n_i}{n_{methanol} + n_{CO}} \tag{5}$$

$$\text{Yield, } Y_i(\%) = \frac{(X_{CO_2} \times S_i)}{100} \tag{6}$$

$$\text{Space time yield, } STY_i\ (g_{methanol}/g_{cat} \cdot h) = \frac{(F_{CO_2} \times M_i \times Y_i)}{V_m \times W_{cat}} \tag{7}$$

where n denotes the number of moles, i represents the product (CH_3OH or CO), F_{CO_2} is the volumetric flow rate of CO_2, M_i denotes the molecular weight of product i, Y_i is the yield of product i, V_m represents the molecular volume of ideal gas at STP (22.414 L/mol) and W_{cat} is the weight of the catalyst.

To elucidate the enhancing effect of ZrO_2 support on the catalytic performance of the catalyst, unsupported In_2O_3 was synthesized by citric acid-based sol-gel method and its catalytic activity in CO_2 hydrogenation reaction was compared to that of In_2O_3/ZrO_2 catalysts. A stability test was conducted using the best performing In_2O_3/ZrO_2 catalyst for 100 h on stream.

4. Characterization Techniques

The surface morphology of the developed catalysts was studied by scanning electron microscopy (SEM) (Zeiss Supra 35VP). The SEM was equipped with energy dispersive X-Ray spectroscopy (EDX) to show the elemental distribution on the surface of the catalysts. High resolution transmission electron microscopy (HR-TEM, Philips CM12 operated at 120 kV) was carried out to observe

the structure of the developed catalysts and mapping was performed to see the dispersion of elements over the catalyst surface. To investigate the crystalline structure of the catalysts, X-ray diffraction (XRD) spectra were recorded on an X' Pert PRO MPD diffractometer with Cu target Kα radiation. The size of crystals was obtained using the Scherrer equation:

$$\text{Crystallite size, } D(\text{nm}) = \frac{k \times \lambda}{\beta \times \cos\theta} \quad (8)$$

where k is a dimensionless shape factor (0.89 assuming spherical shape), λ represents the X-ray wavelength (0.154060 nm), β is full-width-at-half-maximum (FWHM) of diffraction peak in radian and θ is the diffraction angle.

The surface area and pore characteristics data were obtained via N_2 adsorption-desorption isotherms using Autosorb-1-MP instrument (Quantachrome, USA) at −196 °C. The surface area was calculated using Brunauer-Emmett-Teller (BET) model, while pore volume and size were calculated using Barrett-Joyner-Halenda (BJH) method. The redox properties of the developed catalysts were studied by H_2-temperature programmed reduction (H_2-TPR) and CO_2-temperature programmed desorption (CO_2-TPD) experiments. The TPR-TPD tests were carried out in a Micromeritics Autochem II-2920 apparatus following the method described in the literature [8]. To determine the oxidation states of indium and its concentration on the surface, X-Ray photoelectron spectroscopy (XPS) was conducted using AXIS Ultra DLD XPS, Kratos, equipped with monochromatic Al Ka X-ray source.

RESULTS AND DISCUSSION

The catalytic performance and activity of the In_2O_3/ZrO_2 catalysts synthesized through different methods were evaluated in CO_2 hydrogenation reaction. Fig. 1 shows the result for CO_2 conversion, methanol selectivity, yield and STY obtained using the In_2O_3/ZrO_2 catalysts prepared by the three different methods; the average values are summarized in Table 1. All the three In_2O_3/ZrO_2 catalysts exhibited almost similar performance in terms of methanol selectivity with average values in the range of 94.39 to 96.16% (Table S1). The high selectivity achieved using the developed catalysts indicates that the RWGS reaction, the competitive reaction with methanol synthesis, was considerably inhibited by the In_2O_3 catalysts. This result is consistent with DFT studies [9] predicting that the dissociation of CO_2 to CO on defective In_2O_3/ZrO_2 catalyst surface is both energetically and kinetically unfavorable. However, there were significant differences in CO_2 conversion and STY of methanol among the catalysts. The In_2O_3/ZrO_2(SG) catalyst showed the highest CO_2 conversion (16.23%) and STY of methanol (0.95 $g_{methanol}/g_{cat}$·h) among the three catalysts. The CO_2 conversion and STY of methanol obtained using the In_2O_3/ZrO_2(UH) and In_2O_3/ZrO_2(WI) catalysts were 12.76 and 4.46% and 0.66 and 0.28 $g_{methanol}/g_{cat}$·h, respectively. To show the effect of ZrO_2 support on the catalytic activity, the performance of the In_2O_3/ZrO_2 catalyst was compared to that of bulk In_2O_3 prepared by citric acid-based sol-gel method, denoted as bulk In_2O_3. The selectivity of this catalyst (95.56%) was comparable to that of supported catalysts. Nevertheless, its CO_2 conversion (6.99%), methanol yield (6.68%) and STY of methanol (0.44 $g_{methanol}/g_{cat}$·h) were considerably lower than those obtained by In_2O_3/ZrO_2(SG) and In_2O_3/ZrO_2(UH) catalysts. Generally, use of a support can improve the physicochemical properties of the catalyst, which is crucial for catalysis such as providing active clusters and acid-base properties [10]. Enhancement of catalytic performance in case of ZrO_2-supported In_2O_3 compared to the bulk In_2O_3 could be attributed to the better dispersion of metal on the carrier and preventing the sintering of the In_2O_3 during the reaction [7]. It is also plausible that the vacancies contained in the ZrO_2 may be involved in the reaction mechanism where more oxygen vacancies can provide more sites for CO_2 to react with hydrogen, thereby increasing the yield of methanol. Based on theoretical study [9], such improvement can also be associated with supressing the dissociation of CO_2 to CO and higher adsorp-

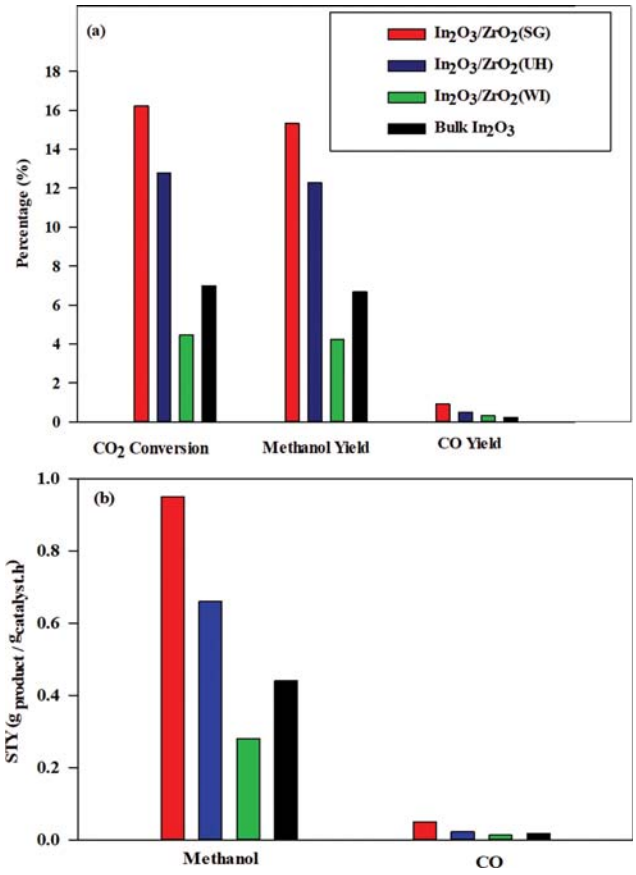

Fig. 1. Catalytic performance of In_2O_3/ZrO_2 catalysts prepared by different synthesis routes in terms of (a) CO_2 conversion and product yield and (b) STY.

Table 1. Structural properties of In_2O_3/ZrO_2 catalysts prepared by different methods

Catalysts	ZrO_2 crystallite size* (nm)	BET surface area (m^2/g)
In_2O_3/ZrO_2(SG)	9	8.9
In_2O_3/ZrO_2(UH)	17	9.9
In_2O_3/ZrO_2(WI)	12	5.8

*Calculated based on the (111) reflection of ZrO_2.

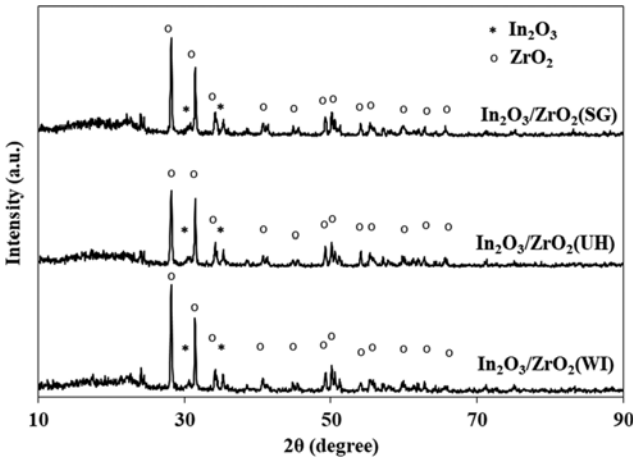

Fig. 2. XRD patterns of the In_2O_3/ZrO_2 catalysts.

tion of the intermediates involved in the reaction for methanol synthesis [11]. The performance of the bulk In_2O_3 catalyst however, outperformed the In_2O_3/ZrO_2(WI) catalyst, which showed a poor catalytic performance. This may denote the effectiveness of the citric acid-based sol-gel method for the development of catalysts with enhanced physicochemical properties. Similar finding was reported by Numpilai et al. [12] who observed that bulk In_2O_3 showed higher methanol yield at 320 °C compared to ZrO_2 supported In_2O_3 prepared by incipient wetness impregnation method.

To explain the differences in the catalytic performance of the In_2O_3/ZrO_2 catalysts prepared by different synthesis methods, several structural characterization analyses were carried out on the catalysts. The characterization results provide useful information to unravel the structure-function relationship. The crystalline structure of the In_2O_3/ZrO_2 catalysts was investigated by XRD analysis and the results are presented in Fig. 2. All catalysts showed almost similar XRD patterns. The diffraction peaks for In_2O_3 appeared at 2θ angle of 30.5° and 35.5° assigning to the diffraction from (222) and 400 plane, which is characteristic of the cubic phase of In_2O_3 [JCPDS card 6-0416]. The peaks located at 2θ values of 28.2° and 31.4° were attributed to the (111) diffraction planes, which indicates the monoclinic structure of ZrO_2 [JCPDS card 01-083-0942]. Monoclinic structure of ZrO_2 is said to be more active than other types due to higher concentration of active intermediates, and Jung and Bell suggested that the monoclinic ZrO_2 may encourage binding the active intermediates [13]. The average crystallite size of In_2O_3 and ZrO_2 was calculated according to the Scherrer equation, and the results are summarized in Table 1. The calculation of the crystallite size was based on the (111) reflection of ZrO_2 in the XRD patterns. Due to the small amount of In_2O_3 loading and well-dispersed particles of In_2O_3 on ZrO_2 support, the FWHM was difficult to determine for In_2O_3, hence it was not considered for the crystallite size calculation. FWHM was obtained using X'Pert Highscore analytical software.

The crystallite size of the catalysts followed the order In_2O_3/ZrO_2(UH)>In_2O_3/ZrO_2(WI)>In_2O_3/ZrO_2(SG). Results indicated that the crystallite size of In_2O_3/ZrO_2(SG) was considerably lower than that prepared by other methods. The superior performance of this catalyst can be attributed to the fact that catalysts with lower crystallite size have higher number of open planes and sites containing unsaturated atoms which are more reactive. More reactive atoms are highly beneficial in terms of stabilizing the key intermediates and capability to reduce the barrier of the rate-limiting dioxymethylene (H_2COO) hydrogenation, as an intermediate of the CO_2 hydrogenation reaction [14]. The unsaturated surface sites often demonstrate stronger adsorption of reactants, intermediates and products. Although the crystallite size of In_2O_3/ZrO_2(UH) was larger than that of In_2O_3/ZrO_2(WI), yet the catalyst prepared via UH presented much better catalytic performance compared to the one synthesized by WI (Table S1). The results obtained from the XRD analysis indicate that crystallite size can influence the catalytic activity, but it is not the main factor for the best catalytic performance of In_2O_3/ZrO_2 in CO_2 hydrogenation to methanol. As discussed in many studies, the synthesis of methanol from CO_2 is very sensitive to the structure of the catalyst, yet it cannot be limited to the crystallite size. Silaghi et al. [15] observed that the CO_2 dissociation process at the metal-support interface was accelerated at optimized metal crystallite size, and the smaller crystallite size did not necessarily provide better catalytic performance. Karelovic et al. [16] also observed a decreasing trend in catalytic activity with smaller crystallite size of Cu catalyst. The high catalytic activity was found to be related the presence of special surface sites which formed some amount of exposed Cu. Thus, it is important to develop catalyst with optimum crystallite size that has a higher number of exposed active surfaces available for the reaction to occur.

The surface area characteristics of the developed In_2O_3/ZrO_2 catalysts are summarized in Table 1. The N_2 adsorption-desorption isotherms (Fig. S3) showed type III isotherm with H_3 hysteresis loop for all the three catalysts, which can correspond to broad distribution of pore size according to IUPAC classification. The surface areas of the catalysts prepared by citric acid-based sol-gel (8.9 m^2/g), deposition-precipitation assisted by urea hydrolysis (9.9 m^2/g) and wetness impregnation (5.8 m^2/g) methods were comparable. This indicates that the preparation method did not have significant effect on the surface area and porosity characteristics of the catalysts. Although it was expected that the catalyst with larger BET surface area possess smaller crystal size, however such correlation was not observed in case of In_2O_3/ZrO_2(UH) and In_2O_3/ZrO_2(WI). According to the literature, in cases where the catalyst particles agglomerate, the correlation between particle size and BET surface area will not be accurate [17]. Also, when the crystallites are embedded into larger structures, the relationship between BET surface area and crystallite size is not necessarily direct [18]. As will be discussed in the following, the results of TEM and SEM analyses indicated the occurrence of agglomeration in In_2O_3/ZrO_2(UH) and to a minor extent in In_2O_3/ZrO_2(WI), which could be the main reason for the observation that particle size was not linked to the BET surface area.

HR-TEM analysis was used to visualize the crystal structure and lattice property of the catalyst. Fig. 3 shows the HR-TEM images of the In_2O_3/ZrO_2 catalysts prepared by different methods. The HR-TEM image of In_2O_3/ZrO_2(SG) clearly shows the lattice fringes with interplanar distance of 0.29 nm corresponding to the (222) plane of In_2O_3. The image also visualizes the (111) plane of ZrO_2

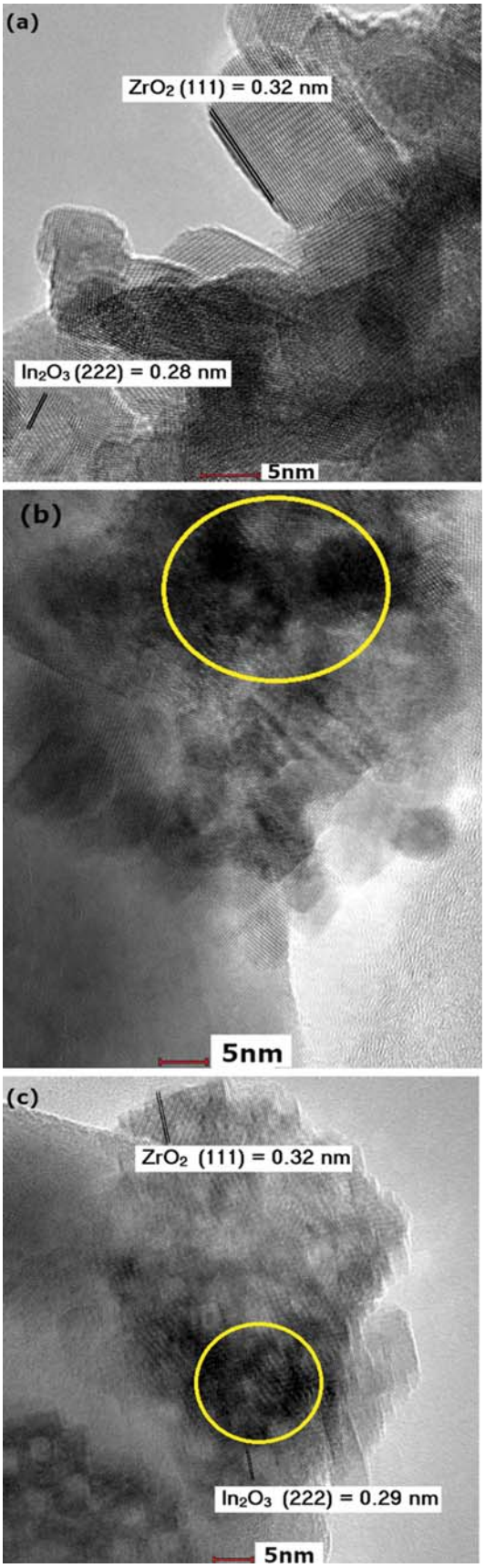

Fig. 3. HR-TEM images of (a) In_2O_3/ZrO_2(SG), (b) In_2O_3/ZrO_2(UH) and (c) In_2O_3/ZrO_2(WI).

with interplanar distance of 0.32 nm. These results are in good agreement with the dominant peaks of In_2O_3 and ZrO_2 obtained from the XRD analysis; this indicates the intimate mixing of cubic

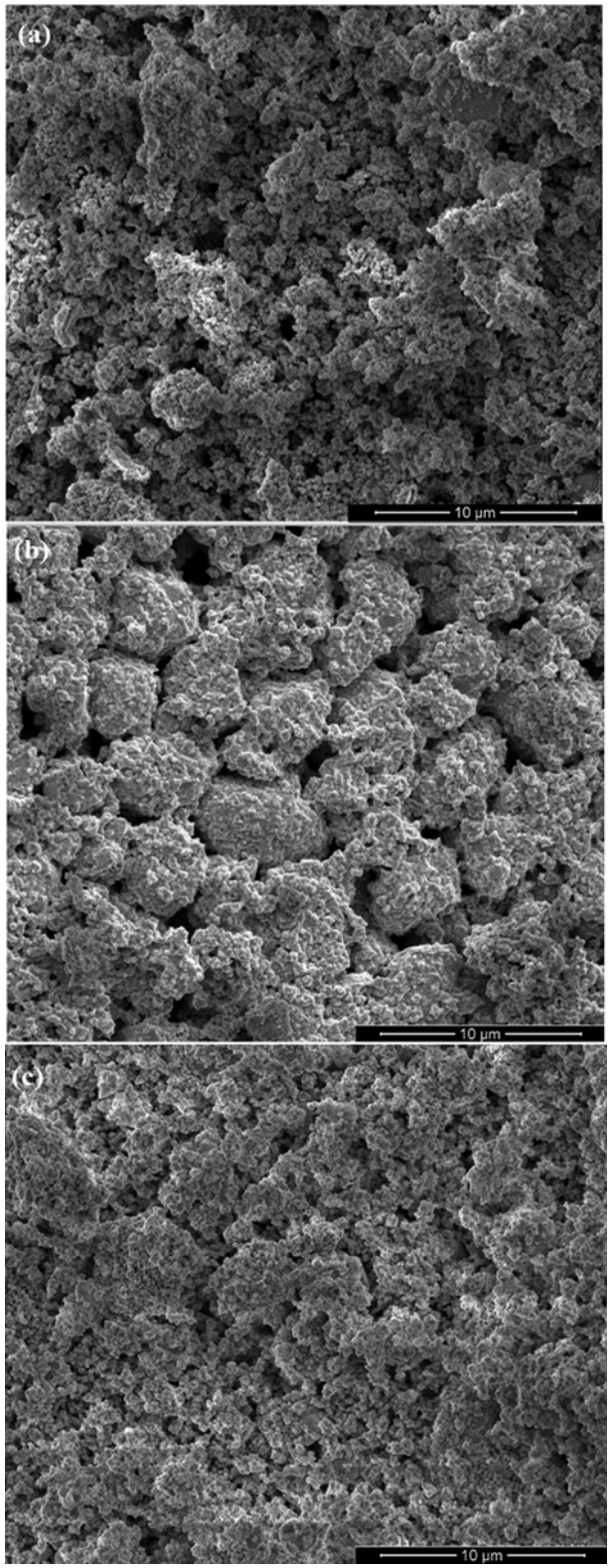

Fig. 4. SEM images of (a) In_2O_3/ZrO_2(SG), (b) In_2O_3/ZrO_2(UH) and (c) In_2O_3/ZrO_2(WI).

In_2O_3 and monoclinic ZrO_2. In_2O_3/ZrO_2(SG) exhibited more exposed surface and more dispersed particles arrangement, while In_2O_3/ZrO_2(UH) showed thicker layers of catalyst, which can be observed as darker spots in the corresponding images. The lattice spacing in In_2O_3/ZrO_2(UH) could not be easily determined due to the indistinct lattice pattern. The darker spots (circled) in TEM image of In_2O_3/ZrO_2(UH) could be associated with agglomeration, which reduces the availability of active sites for CO_2 adsorption on the In_2O_3 surface. Despite the smaller single crystallite size of In_2O_3/ZrO_2(WI) compared to In_2O_3/ZrO_2(UH), Fig. 3(c) shows that agglomeration possibly occurred at some areas of this catalyst, as evidenced by clump formation (circled). The TEM elemental mapping (Fig. S4) provides information on dispersion of elements on the surface of the developed catalysts. In_2O_3/ZrO_2(SG) presented a uniform dispersion of In_2O_3 on the ZrO_2 support. The mapping of In_2O_3/ZrO_2(UH) indicated spots with high intensity of In which could be correlated with the formation of aggregates during catalyst preparation. The elemental mapping of In_2O_3/ZrO_2(WI) evidenced the uniform, yet low presence of In_2O_3 on the ZrO_2 support. These results are consistent with those obtained from SEM images (Fig. 4). It can be clearly observed from Fig. 4 that In_2O_3/ZrO_2(WI) formed small size particles, but the particles were more closely packed to each other compared to the In_2O_3/ZrO_2(SG) catalyst. The elemental mapping results (Fig. S4 and S5) showed surface agglomeration and high surface concentration of In (13.75%) in case of the In_2O_3/ZrO_2(UH) catalyst, while the surface concentration of In on the In_2O_3/ZrO_2(WI) catalyst was quite low (3.27%), which shows the low dispersion of In_2O_3 on the ZrO_2 support. Agglomeration leads to the formation of larger particles, which can reduce the exposure of the active phase of the catalyst with reactants. In contrast, the better catalytic performance of In_2O_3/ZrO_2(SG) can also be attributed to the uniform dispersion of In_2O_3 on the support. Uniformly distributed and highly dispersed active metals play a crucial role in catalysis. Higher dispersion of catalyst on the support provides more available active sites for the reaction to occur. Evidently, Allam et al. [19] showed that the better dispersion of CeO_2 supported catalysts prepared by polyol method improved the catalytic performance in terms of CO_2 conversion and methanol selectivity due to the presence of sufficient active sites for the reaction to occur. Ouyang et al. [20] indicated that different catalyst preparation methods affect the catalyst morphology. They also discussed that high metal oxide dispersion with less aggregation is necessary to achieve high CO_2 conversion to methanol. The higher dispersion of InO_3 on ZrO_2 support augments the capability of CO_2 adsorption on the catalyst surface, thus enhancing the CO_2 hydrogenation reaction.

The reduction temperature of supported In_2O_3 gives information about the strength of interaction between the catalyst and the support. The strength of metal-support interaction can be implied by the different reduction temperature profiles of each catalyst. The shift of the H_2 consumption peak towards higher reduction temperatures can be regarded as a stronger interaction between metal and support. The metal-support interaction can be related to the reducibility of the catalyst, where at lower reduction temperatures the catalyst is considered to be highly reducible. To study the reduction behavior of the synthesized catalysts, TPR reaction was carried out in hydrogen; the profiles of H_2 consumption are exhibited in Fig. 5. From the figure, the highest peak for bulk In_2O_3 was observed at 546 °C. When In_2O_3 was supported on ZrO_2, the peak shifted towards higher temperature, which indicates that the interaction between In_2O_3 and ZrO_2 was induced. Three major peaks can be seen for In_2O_3/ZrO_2(SG) and In_2O_3/ZrO_2(UH), while only two major peaks were detected for In_2O_3/ZrO_2(WI). The peaks observed at 99.7 and 107 °C for In_2O_3/ZrO_2(UH) and In_2O_3/ZrO_2(SG), respectively, could be attributed to the production of $(InO)^+$, which was easily reducible and was also associated with the active species for the hydrogenation reaction to methanol [21]. The $(InO)^+$ formation peak, however, did not present in In_2O_3/ZrO_2(WI) and bulk In_2O_3. More intense reduction peaks appearing between 583 to 695 °C for all catalysts were attributed to the reduction of bulk In_2O_3 [22]. The peaks at temperature higher than 707 °C, which is absent in the H_2-TPR profile of bulk In_2O_3, could be associated with the reductive exchange that occurred between In_2O_3 and ZrO_2. The highest reduction temperature (695 °C) was required to reduce the catalyst prepared by WI method. The catalysts prepared by UH (562 °C) and SG (583 °C) methods and also the bulk In_2O_3 (546 °C) revealed reduction peaks at lower temperatures compared to the one synthesized by WI. This suggests that addition of urea and citric acid was effective to shift the peaks towards lower temperatures. In fact, urea and citric acid could enhance the reducibility of the catalysts, which has a great impact on the catalytic performance, thus making it more accessible towards H_2 'attack' [23]. Accordingly, H atoms can affect the catalytic performance either by direct reaction with activated CO_2 or reduction of In_2O_3 surface to create more oxygen vacancies, which is beneficial for the synthesis of methanol from H_2 and CO_2 [24]. Studies show that catalysts with lower reduction temperature provide higher yield of methanol and productivity [25,26]. In this study, In_2O_3/ZrO_2(WI), which revealed higher reduction temperature, had lower catalytic activity compared to the other two catalysts. The catalysts prepared by citric acid-based

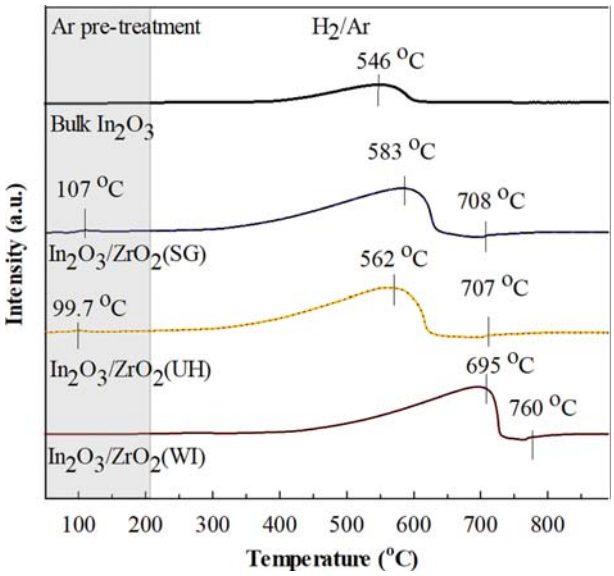

Fig. 5. H_2-TPR profiles of the In_2O_3/ZrO_2 catalysts synthesized by different methods.

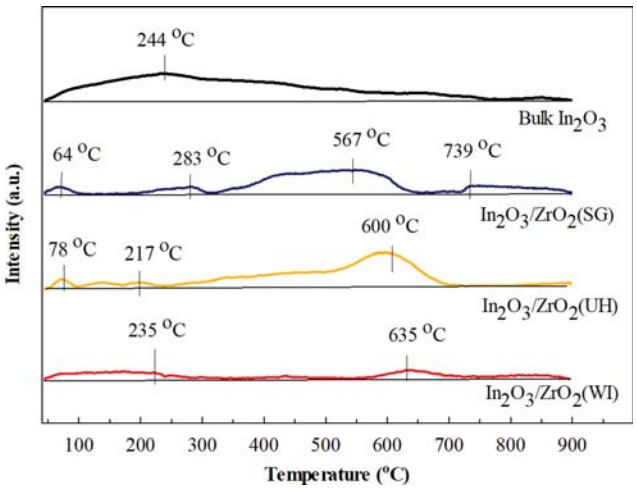

Fig. 6. CO_2-TPD profiles of the In_2O_3/ZrO_2 catalysts synthesized by different methods.

sol-gel method and the one synthesized by deposition-precipitation assisted by urea hydrolysis method showed comparable reducibility profile, yet the performance of the former was better than the latter. This signifies that beside reducibility, other physicochemical parameters such as crystallite size, porosity, and surface basicity contribute to the activity and performance of the catalyst.

The basicity of the synthesized catalysts was determined by CO_2-TPD analysis. The degree of basicity of the catalyst sites gives information on strength of CO_2 bond on the catalyst surface and can suggest which sites are more favorable for the reaction [22]. Fig. 6 illustrates the CO_2 desorption curves of the catalysts in the range of 100 to 900 °C. The CO_2 desorption profile temperature could be divided into three categories: weak basic sites (<200 °C), moderate basic sites (200 to 650 °C) and strong basic sites (>650 °C). Weak basic site is associated with surface hydroxyl group (OH^-), while moderate basic site is related to metal-oxygen (M^{n+}-O^-) interaction where n is the number of ion; the strong basic site represents the low coordination of unsaturated oxygen (O^{2-}) with electronegative ions [27]. According to the CO_2 desorption profile of In_2O_3/ZrO_2(SG), four desorption peaks were detected. One peak was detected in weak temperature region (64 °C), two in moderate temperature region (283 and 567 °C) and one in high temperature region (739 °C). The In_2O_3/ZrO_2(UH) catalyst represented three distinct peaks in low (78 °C) and medium (217 and 600 °C) temperature regions, respectively, assigned to weak and medium basic sites. While, the CO_2-TPD curve of In_2O_3/ZrO_2(WI) exhibited only two broad peaks at medium (235 and 638 °C) temperature region. The In_2O_3/ZrO_2(SG) catalyst revealed two peaks corresponding to moderate basic sites. This indicates that more CO_2 can be adsorbed at moderate range of basicity. Also, in case of this catalyst, the desorption peak corresponding to strong basic sites appeared in higher temperature region compared to the other two catalysts, suggesting that the strength of its basic sites is higher. This could be attributed to the increase of electron density of the strong basic sites by the aggregation of saturated O^{2-} ions [28]. The peaks at high temperature range could be associated with stronger binding of CO_2 on the catalyst surface, which could enhance the formation of methanol [29]. The peak detected at weak basic sites also corresponds to the physically adsorbed CO_2. Based on the intensity of the peaks associated with weak basic sites, more CO_2 was adsorbed on In_2O_3/ZrO_2(UH) followed by In_2O_3/ZrO_2(SG) and no peak was detected for In_2O_3/ZrO_2(WI) and bulk In_2O_3 indicating the weak capability of these catalysts to adsorb CO_2 at weak basic sites. However, the capability of the catalyst to physically adsorb CO_2 at weak basic sites is not the only factor that affects the catalytic performance. Based on the study by Ud et al. [30], the existence of the basic sites at various ranges of basicity is beneficial to improve the catalytic performance. In our case, the excellent performance of In_2O_3/ZrO_2(SG) could be due to the ability of the catalyst to adsorb CO_2 in wider range of basic sites. It could also correspond to the higher number of basic sites available in this catalyst that resulted in higher total amount of CO_2 adsorption (Table 2). The values of CO_2 basic strength in Table 2 were acquired using a developed calibration curve of the TCD signal peak area against the partial pressure of the injected CO_2.

The CO_2-TPD profile also gives information on the oxygen vacancy formation. Rui et al. [24] mentioned that medium and strong basic site regions can be correlated with the formation of oxygen vacancies which are the active sites for CO_2 hydrogenation to methanol. From the CO_2 adsorption values in Table 2, it can be inferred that more oxygen vacancies were formed in In_2O_3/ZrO_2(SG) followed by In_2O_3/ZrO_2(UH), bulk In_2O_3 and In_2O_3/ZrO_2(WI). The better catalytic performance of bulk In_2O_3 over the In_2O_3/ZrO_2(WI) catalyst could be due to its higher concentrations of medium and strong basic sites (Table 2) and thus its ability to adsorb more CO_2 and also formation of higher concentration of oxygen vacancies, which play a significant role in CO_2 hydrogenation to methanol.

The oxidation state and oxygen deficiency were analyzed using XPS analysis. Fig. 7(a) shows the characteristics of In $3d_{5/2}$ and In $3d_{3/2}$ signals. The spin-orbit splitting between the two peaks was around the standard value of 7.6 eV, indicating the presence of In^{3+} in the samples. The intensity of the peak for In_2O_3/ZrO_2(SG) was

Table 2. CO_2-TPD quantitative data

Catalyst	CO_2 desorption at basic sites with different strengths (mmol/g_{cat})			
	Weak basic sites	Medium basic sites	Strong basic sites	Total basic sites
In_2O_3/ZrO_2(SG)	1.7	13.4	1.1	16.2
In_2O_3/ZrO_2(UH)	2.1	4.9	-	7.0
In_2O_3/ZrO_2(WI)	-	5.8	-	5.8
Bulk In_2O_3	-	6.5	0.6	7.1

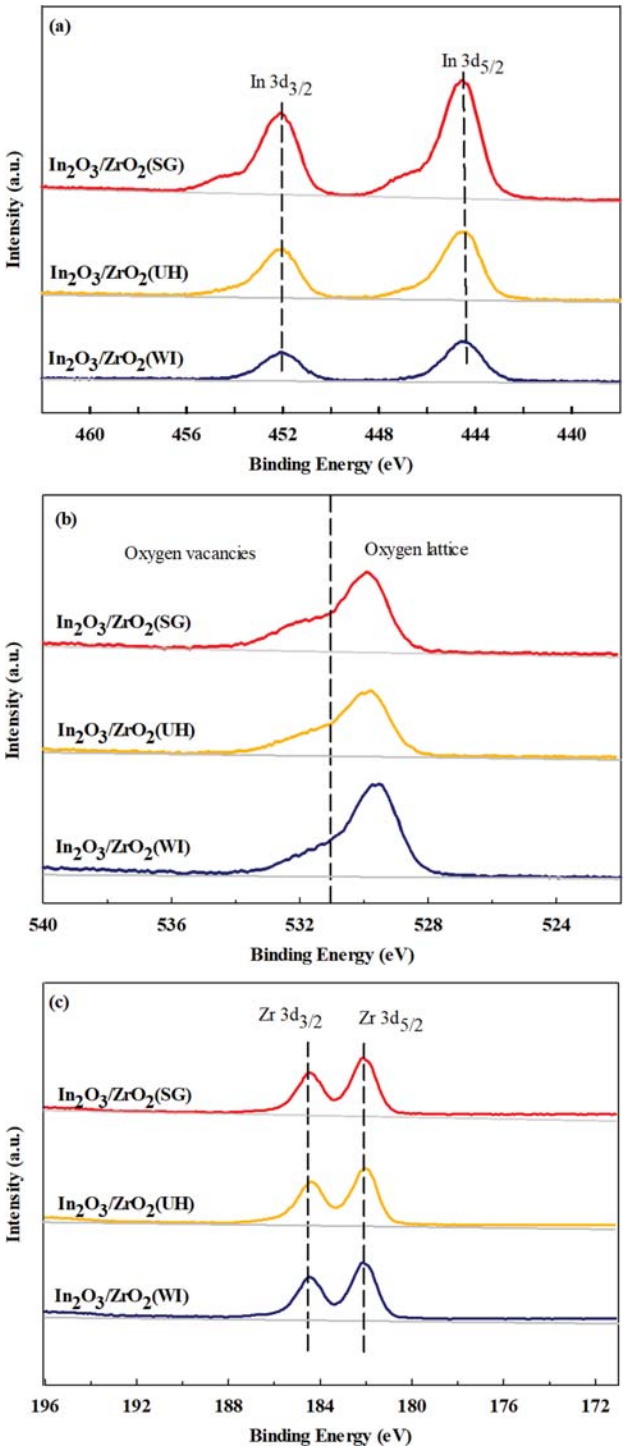

Fig. 7. XPS spectra of (a) In 3d, (b) O 1s and (c) Zr 3d of In_2O_3/ZrO_2 catalysts.

highest compared to In_2O_3/ZrO_2(UH) and In_2O_3/ZrO_2(WI) due to the presence of more In^{3+} in the sample, which implies that there were more oxygen defects in this catalyst.

A detailed configuration of O 1s core level spectra is represented in Fig. 7(b). The peaks at about 530 eV can be indexed to the lattice oxygen ($O_{lattice}$), while the peaks observed at higher binding energy of 532 eV correspond to the defective oxygen region (O_{defect})

Table 3. XPS peak intensity ratio of In $3d_{5/2}$/Zr $3d_{5/2}$

Catalyst	Peak intensity ratio
In_2O_3/ZrO_2(SG)	2.58
In_2O_3/ZrO_2(UH)	1.59
In_2O_3/ZrO_2(WI)	1.15

[31]. It can be observed that the peak area of defective oxygen in In_2O_3/ZrO_2(SG) is wider, which indicates that more oxygen vacancies are available for CO_2 adsorption on the In_2O_3 surface. The concentration of surface oxygen vacancy was calculated using the peak area (A) of different oxygen species based on the formula $C_{Odefect}=A_{Odefect}/(A_{Odefect+}A_{Olattice})$ [24]. The concentration of oxygen vacancies was calculated as 30, 25 and 20% for In_2O_3/ZrO_2(SG), In_2O_3/ZrO_2(UH) and In_2O_3/ZrO_2(WI), respectively. Higher amount of this defective oxygen allowed more CO_2 to be adsorb on the catalyst surface for the reaction with H_2 adatoms. The creation of oxygen vacancies is crucial for CO_2 hydrogenation to methanol in order to provide more sites for CO_2 adsorption on the catalyst surface. The creation of oxygen vacancies can be encouraged if the catalysts have good ability to dissociatively adsorb hydrogen, thereby supplying more hydrogen for CO_2 hydrogenation stages [24].

Fig. 7(c) shows the Zr 3d spectra for the three catalysts prepared by different methods. The binding energy values which range between 182.2 and 182.3 eV for Zr $3d_{5/2}$ and 184.4 and 184.6 eV for Zr $3d_{3/2}$ are in good agreement with the literature [32,33]. The deconvolution of the spin-orbit doublet reflects the presence of Zr^{4+}. The spectrum of Zr 3d revealed two peaks representing Zr^{4+} in ZrO_2 lattice and Zr^{4+} in an electrophilic surrounding likely to bond with hydroxyl group [34]. No Zr^{3+} was detected in the catalyst, which means that ZrO_2 was not reduced after the pre-treatment. The ZrO_2 support is assumed to facilitate the conversion of the adsorbed CO_2 to formate or hydroxylcarbonyl species. Formate species is the most important intermediate and the In_2O_3/ZrO_2 interface is important for the conversion of the intermediates to methanol [35]. The interaction that exists between In_2O_3 and ZrO_2 not only encourages the oxygen vacancy creation but also prevents the sintering at In_2O_3 phase [36]. Peak intensity ratio of active metals over supports can provide useful information about the dispersion of metal on the support. From the results summarized in Table 3, it can be inferred that higher peak intensity ratio of In_2O_3/ZrO_2(SG) could be an indication of better dispersion of In_2O_3 on the ZrO_2 support followed by In_2O_3/ZrO_2(UH) and In_2O_3/ZrO_2(WI). The better dispersion of In_2O_3 in the In_2O_3/ZrO_2(SG) catalyst could cause more adsorption of the reactants on the active sites, hence improving the catalytic activity of the catalyst. Chary et al. [37] also discussed that the decrease in the metal oxide support peak intensity could result from the formation of larger crystallites, which is in agreement with the XRD results presented in this study.

Characterization results indicated that the superior performance of In_2O_3/ZrO_2(SG) over other catalysts was attributed to its smaller crystallite size, uniform dispersion of metal on the support, higher reducibility, stronger surface basicity with higher number of basic sites and higher concentration of oxygen vacancies on the surface. The better catalytic performance of In_2O_3/ZrO_2(SG) could also be due to the presence of COOH group from citric acid [38]. The che-

lation reaction between cations and alpha-carboxylic acid of citric acid allows the formation of a very stable chelating complex with metal ions. Citric acid is known to provide polymeric network that can hinder the cation mobility, hence maintaining the local stoichiometry which cannot be provided by deionized water (in WI method) and amide group of urea (in UH method) [39]. Although all catalysts were developed using the same nominal concentration of In_2O_3 (10 wt%), the presence of citric acid as chelating agent in In_2O_3/ZrO_2(SG) could modify the chemical properties of the catalyst, thus improving its catalytic performance for CO_2 hydrogenation to methanol. In addition, our results indicated that the performance of the catalyst in this reaction was structure-dependent, where any minor modification during catalyst preparation could give a significant impact on the catalytic activity. This was associated with the effect of catalyst synthesis method on the physicochemical properties, including crystallite size, metal dispersion, surface basicity and metal-support interactions. Apart from morphological properties, the different preparation methods could also contribute to the formation of oxygen vacancies and improved reducibility of the catalysts, which would provide more active sites for the CO_2 hydrogenation reaction.

The long-term stability of the bulk In_2O_3 and In_2O_3/ZrO_2(SG) catalyst in CO_2 hydrogenation reaction was tested over 100 h on stream. In_2O_3/ZrO_2 was able to sustain its high $STY_{methanol}$ (0.95 to 0.97 $g_{methanol}/g_{cat}$·h) during the first 82 h, while the activity of unsupported bulk In_2O_3 reduced gradually every hour (Fig. 8). During the 10 h of run, the catalyst selectivity remained almost unchanged between 94-96% for In_2O_3/ZrO_2. Then, a gradual decrease in methanol yield was observed and the $STY_{methanol}$ was reduced by 15% after 100 h. The decrease in catalytic performance could be due to the deactivation of the catalyst contributed by several factors, such as formation of water and production of CO as the side product that can cause catalyst sintering and over-reduction. The high STY of methanol and long-term stability indicate that In_2O_3/ZrO_2(SG) is a potential and stable catalyst for CO_2 hydrogenation to methanol. The performance of this catalyst was comparable to those reported for Cu-based catalysts as summarized in Table 4.

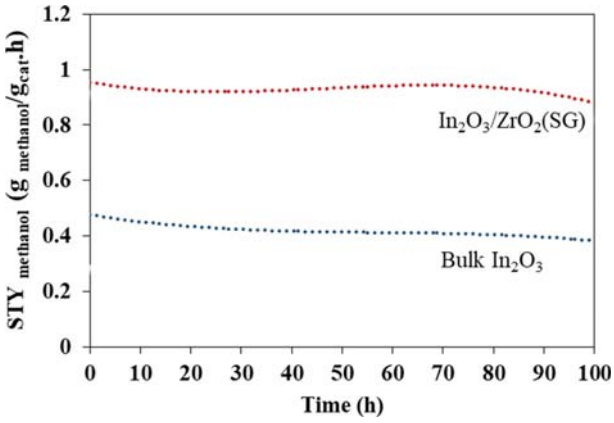

Fig. 8. Catalytic performance of bulk In_2O_3 and In_2O_3/ZrO_2(SG) over 100-h run.

CONCLUSION

This study demonstrates that the catalyst preparation method could affect the structure, and hence influence, the performance of the catalyst. Based on the findings, active metal dispersion on support, strong metal-support interaction, CO_2 adsorption capability at various temperature ranges and higher concentration of oxygen vacancies and reducibility of the catalyst play a significant role in facilitating CO_2 hydrogenation to methanol and mainly affect the CO_2 conversion and methanol yield. In_2O_3/ZrO_2(SG) showed superior catalytic performance compared to the other two catalysts because of its smaller crystallite size, higher reducibility, better dispersion of In_2O_3 on the support, stronger surface basicity and higher concentration of oxygen vacancies on the surface. Regardless of different preparation methods, the methanol selectivity was above 90% for all catalysts, which means that In_2O_3/ZrO_2 is a potential catalyst in CO_2 hydrogenation to methanol. Use of ZrO_2 as support boosted the catalytic performance by acting as a platform for better active metal dispersion and providing improved metal-support interaction based on the H_2-TPR analysis. The In_2O_3/ZrO_2(SG)

Table 4. A survey of literature on catalytic performance of different catalysts in CO_2 hydrogenation reaction

Catalysts	Temperature (°C)	Pressure (MPa)	WHSV (mL/g_{cat}·h)	CO_2 conversion (%)	Methanol selectivity (%)	Methanol yield (%)	Reference
$CuO-ZnO-ZrO_2$	240	3	2,400	19.7	49.3	9.7	[40]
$CuO-ZnO-ZrO_2$	200	2	15,600	2	68	1.36	[41]
In_2O_3/ZrO_2 (prepared by incipient wetness method)	280	3	4,000	6	55	3.3	[22]
In-Co	300	5	14,400	6	25	1.5	[42]
Ni-Sn/In-ZrO_2	250	2.5	40,000	na	95	na	[43]
0.25Cu-0.75In-Zr-O	250	2.5	18,000	1.5	75	1.1	[44]
In_2O_3/ZrO_2 (co-precipitation)	300	5	na	5.2	99.8	5.2	[7]
In_2O_3/ZrO_2	300	4	50,000	11	53	5.83	[45]
$CuO-ZnO-ZrO_2$-2.5 wt% graphene oxide	280	2	n/a	24.8	10	2.5	[46]
In_2O_3/ZrO_2(SG)	280	4	15,000	16.2	94.4	15.3	This work

catalyst also revealed high $STY_{methanol}$ (around 1 $g_{methanol}/g_{cat}$·h) and selectivity (95%), which could be sustained for more than 80 h. These findings signify that In_2O_3/ZrO_2 can be a promising catalyst for direct hydrogenation of CO_2 to methanol with minimum side reactions.

ACKNOWLEDGEMENTS

This work was supported by the Long-Term Research Grant Scheme (LRGS NanoMITe) from Ministry of Education Malaysia [grant number 203/PJKIMIA/6720009]. The authors also gratefully acknowledge the Institute of Scientific and Industrial Research (ISIR), Osaka University for valuable help in HR-TEM imaging.

SUPPORTING INFORMATION

Additional information as noted in the text. This information is available via the Internet at http://www.springer.com/chemistry/journal/11814.

REFERENCES

1. S. G. Jadhav, P. D. Vaidya, B. M. Bhanage and J. B. Joshi, *Chem. Eng. Res. Des.*, **92**, 2557 (2014).
2. C. Temvuttirojn, Y. Poo-Arporn, N. Chanlek, C. K. Cheng, C. C. Chong, J. Limtrakul and T. Witoon, *Ind. Eng. Chem. Res.*, **59**, 5525 (2020).
3. M. F. Hertrich and M. Beller, in: *Met. Hydrog. CO2 into Methanol*, Springer International Publishing, Cham, Switzerland (2018).
4. Y. Zhang, L. Zhong, H. Wang, P. Gao, X. Li, S. Xiao, G. Ding, W. Wei and Y. Sun, *J. CO2 Util.*, **15**, 72 (2016).
5. J. Ye, C. Liu, D. Mei and Q. Ge, *ACS Catal.*, **3**, 1296 (2013).
6. K. Sun, Z. Fan, J. Ye, J. Yan, Q. Ge, Y. Li, W. He, W. Yang and C. J. Liu, *J. CO2 Util.*, **12**, 1 (2015).
7. O. Martin, A. J. Martín, C. Mondelli, S. Mitchell, T. F. Segawa, R. Hauert, C. Drouilly, D. Curulla-Ferré and J. Pérez-Ramírez, *Angew. Chem. Int. Ed.*, **55**, 6261 (2016).
8. M. K. Koh, Y. J. Wong, S. P. Chai and A. R. Mohamed, *J. Ind. Eng. Chem.*, **62**, 156 (2018).
9. M. Zhang, M. Dou and Y. Yu, *Appl. Surf. Sci.*, **433**, 780 (2018).
10. M. Liu, Y. Yi, L. Wang, H. Guo and A. Bogaerts, *Catalysts*, **9**, 275 (2019).
11. M. Dou, M. Zhang, Y. Chen and Y. Yu, *Surf. Sci.*, **672-673**, 7 (2018).
12. T. Numpilai, P. Kidkhunthod, C. K. Cheng, C. Wattanakit, M. Chareonpanich, J. Limtrakul and T. Witoon, *Catal. Today*, in press (2020).
13. K. T. Jung and A. T. Bell, *Catal. Lett.*, **80**, 63 (2002).
14. S. Natesakhawat, J. W. Lekse, J. P. Baltrus, P. R. Ohodnicki, B. H. Howard, X. Deng and C. Matranga, *ACS Catal.*, **2**, 1667 (2012).
15. M. C. Silaghi, A. Comas-Vives and C. Copéret, *ACS Catal.*, **6**, 4501 (2016).
16. A. Karelovic, G. Galdames, J. C. Medina, C. Yévenes and Y. Barra, *J. Catal.*, **369**, 415 (2019).
17. B. Akbari, M. P. Tavandashti and M. Zandrahimi, *Iran. J. Mater. Sci. Eng.*, **8**, 48 (2011).
18. F. Jaouen, F. Charreteur and J. P. Dodelet, in: Carbon Struct. Act. Non-Noble Catal. Oxyg. Reduct. *PEMFC*, 176 (2005).
19. D. Allam, S. Bennici, L. Limousy and S. Hocine, *Comptes Rendus Chim.*, **2-3**, 227 (2019).
20. B. Ouyang, W. Tan and B. Liu, *Catal. Commun.*, **95**, 36 (2017).
21. H. P. Decolatti, A. Martínez-Hernández, L. B. Gutiérrez, G. A. Fuentes and J. M. Zamaro, *Micropor. Mesopor. Mater.*, **145**, 41 (2011).
22. J. Wang, A. Zhang, X. Jiang, C. Song and X. Guo, *J. CO2 Util.*, **27**, 81 (2018).
23. S. Li, Y. Wang, B. Yang and L. Guo, *Appl. Catal. A Gen.*, **571**, 51 (2018).
24. N. Rui, Z. Wang, K. Sun, J. Ye, Q. Ge and C. Liu, *Appl. Catal. B Environ.*, **218**, 488 (2017).
25. N. Le-Phuc, T. V. Tran, P. N. Thuy, L. H. Nguyen and T. T. Trinh, *React. Kinet. Mech. Catal.*, **124**, 171 (2018).
26. G. Wang, D. Mao, X. Guo and J. Yu, *Int. J. Hydrogen Energy*, **44**, 4197 (2019).
27. P. Gao, H. Yang, L. Zhang, C. Zhang, L. Zhong, H. Wang, W. Wei and Y. Sun, *J. CO2 Util.*, **16**, 32 (2016).
28. C. I. Ezeh, X. Yang, J. He, C. Snape and X. M. Cheng, *Ultrason. Sonochem.*, **42**, 48 (2018).
29. N. Akkharaphatthawon, N. Chanlek, C. K. Cheng, M. Chareonpanich, J. Limtrakul and T. Witoon, *Appl. Surf. Sci.*, **489**, 278 (2019).
30. I. Ud, M. S. Shaharun, A. Naeem, S. Tasleem and M. Ra, *Catal. Today*, **21**, 145 (2017).
31. R. R. Krishnan, V. S. Kavitha, S. M. C. Kumar, K. G. Gopchandran and M. V. P. Pillai, *Mater. Sci. Semicond. Process.*, **93**, 134 (2019).
32. Y. Wang, S. Kattel, W. Gao, K. Li, P. Liu, J. G. Chen and H. Wang, *Nat. Commun.*, **10**, 1166 (2019).
33. W. Wang, Z. Qu, L. Song and Q. Fu, *J. Energy Chem.*, **40**, 22 (2020).
34. K. Samson, M. Sliwa, R. P. Socha, K. Góra-Marek, D. Mucha, D. Rutkowska-Zbik, J. F. Paul, M. Ruggiero-Mikoajczyk, R. Grabowski and J. Soczyński, *ACS Catal.*, **4**, 3730 (2014).
35. W. Wang, Z. Qu, L. Song and Q. Fu, *J. Energy Chem.*, **40**, 22 (2020).
36. K. Li and J. G. Chen, *ACS Catal.*, **9**, 7480 (2019).
37. K. V. R. Chary, G. V. Sagar, C. S. Srikanth and V. V. Rao, *J. Phys. Chem. B*, **111**, 543 (2007).
38. A. Rajaeiyan and M. M. Bagheri-Mohagheghi, *Adv. Mater. Sci. Eng.*, **1**, 176 (2013).
39. F. Davar, A. Hassankhani and M. R. Loghman-Estarki, *Ceram. Int.*, **39**, 2933 (2013).
40. G. Wang, D. Mao, G. Xiaoming and Y. Jun, *Appl. Surf. Sci.*, **456**, 403 (2018).
41. T. Phongamwong, U. Chantaprasertporn, T. Witoon, T. Numpilai, P. Yingyot, W. Limphirat, W. Donphai, P. Dittanet, M. Chareonpanich and J. Limtrakul, *Chem. Eng. J.*, **316**, 692 (2017).
42. A. Bavykina, I. Yarulina, A. J. Al Abdulghani, L. Gevers, M. N. Hedhili, X. Miao, A. R Galilea, A. Pustovarenko, A. Dikhtiarenko, A. Cadiau, A. Aguilar-Tapia, J. Hazemann, S. M. Kozlov, S. Oud-Chikh, L.Cavallo and J. Gascon, *ACS Catal.*, **8**, 6910 (2019).
43. A. M. Hengne, A. K. Samal, L. R. Enakonda, M. Harb, L. E. Gevers, D. H. Anjum, M. N. Hedhili, Y. Saih, K. W. Huang and J. M. Basset, *ACS Omega*, **3**, 3688 (2018).
44. L. Yao, X. Xhen, Y. Pan and Z. Peng, *J. Catal.*, **372**, 74 (2019).
45. C. Chou and R. Lobo, *Appl. Catal. A Gen.*, **583**, 117 (2019).
46. T. Witoon, T. Numpilai, T. Phongamwong, W. Donphai, C. Boonyuen, C. Warakulwit, M. Chareonpanich and J. Limtrakul, *Chem. Eng. J.*, **334**, 1781 (2018).

Supporting Information

Development of highly selective In_2O_3/ZrO_2 catalyst for hydrogenation of CO_2 to methanol: An insight into the catalyst preparation method

Munirah Md Zain*, Maedeh Mohammadi, Naoto Kamiuchi***, and Abdul Rahman Mohamed*,†**

*Low Carbon Economy (LCE) Research Group, School of Chemical Engineering, Universiti Sains Malaysia, 14300 Nibong Tebal, Pulau Pinang, Malaysia
**Faculty of Chemical Engineering, Babol Noshirvani University of Technology, 47148 Babol, Iran
***The Institute of Scientific and Industrial Research, Osaka University, 8-1 Mihogaoka, Ibaraki, Osaka 567-0047, Japan
(*Received 9 February 2020 • Revised 4 May 2020 • Accepted 11 May 2020*)

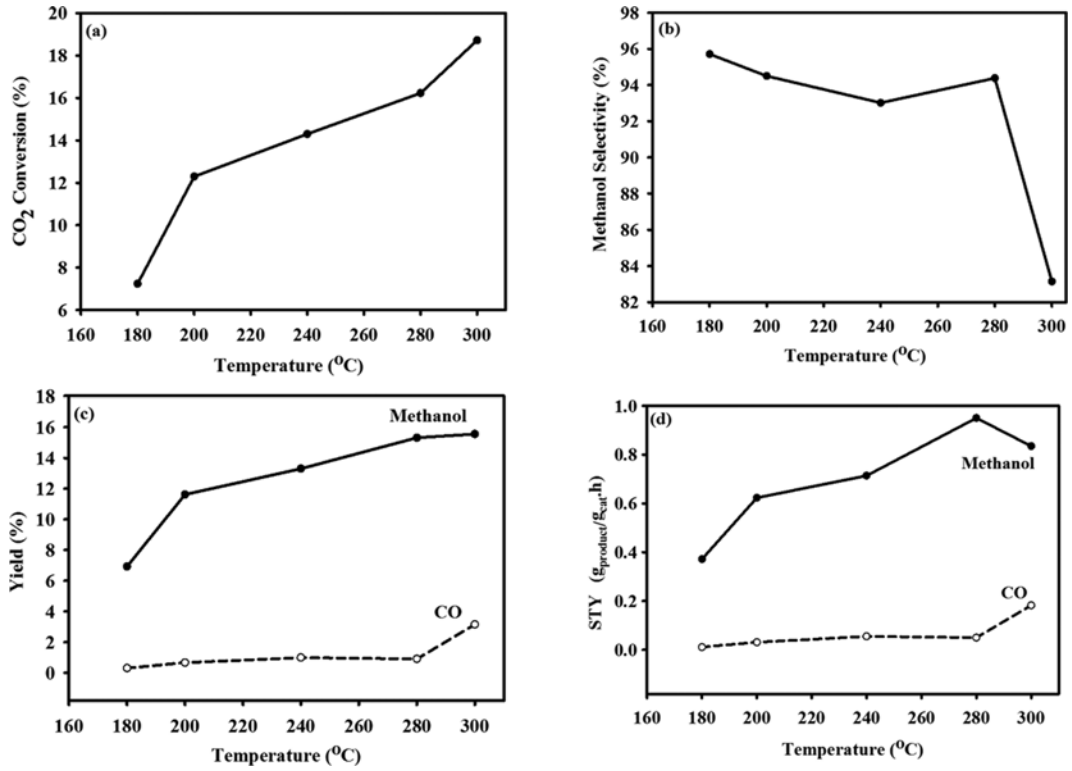

Fig. S1. Catalytic performance of In_2O_3/ZrO_2 at various temperatures.

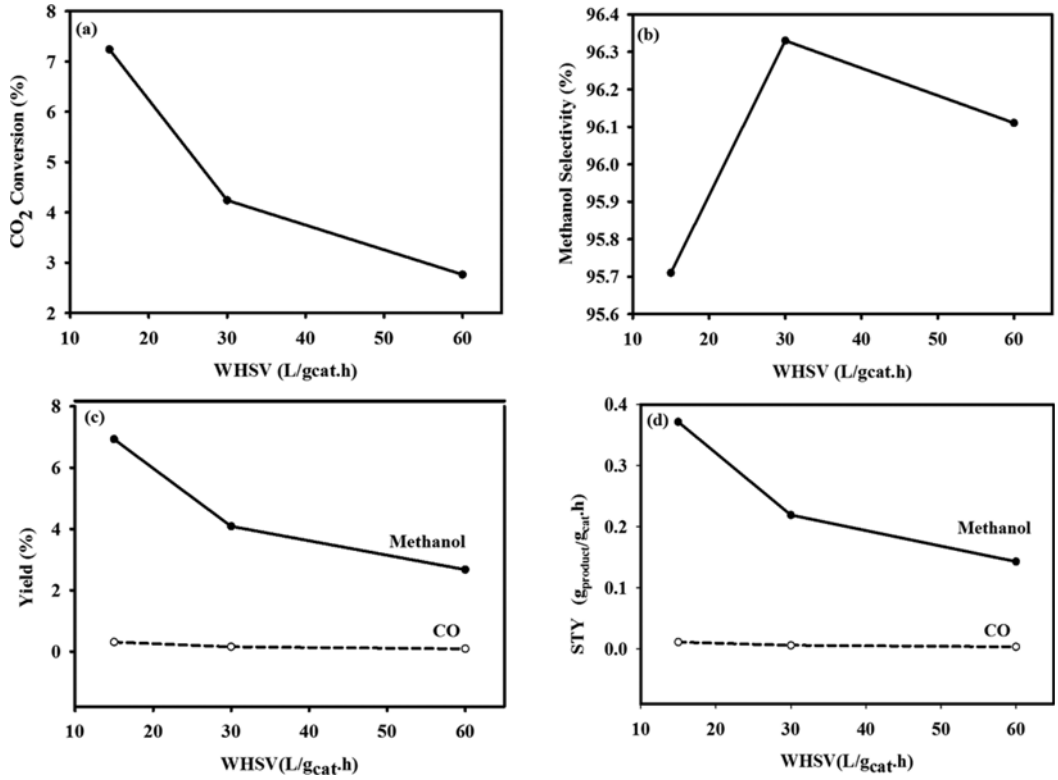

Fig. S2. Catalytic performance of In_2O_3/ZrO_2 at various WHSV.

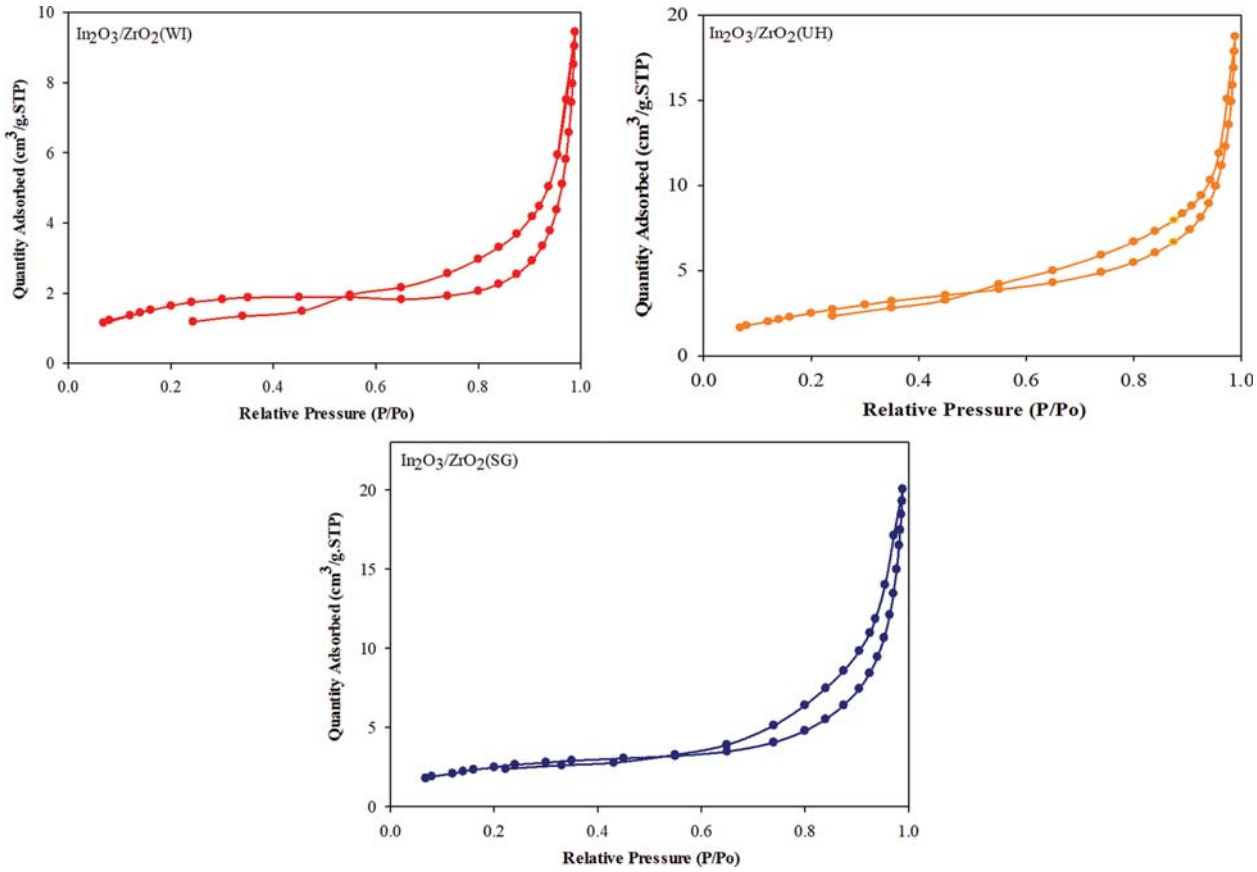

Fig. S3. N_2 adsorption-desorption isotherms.

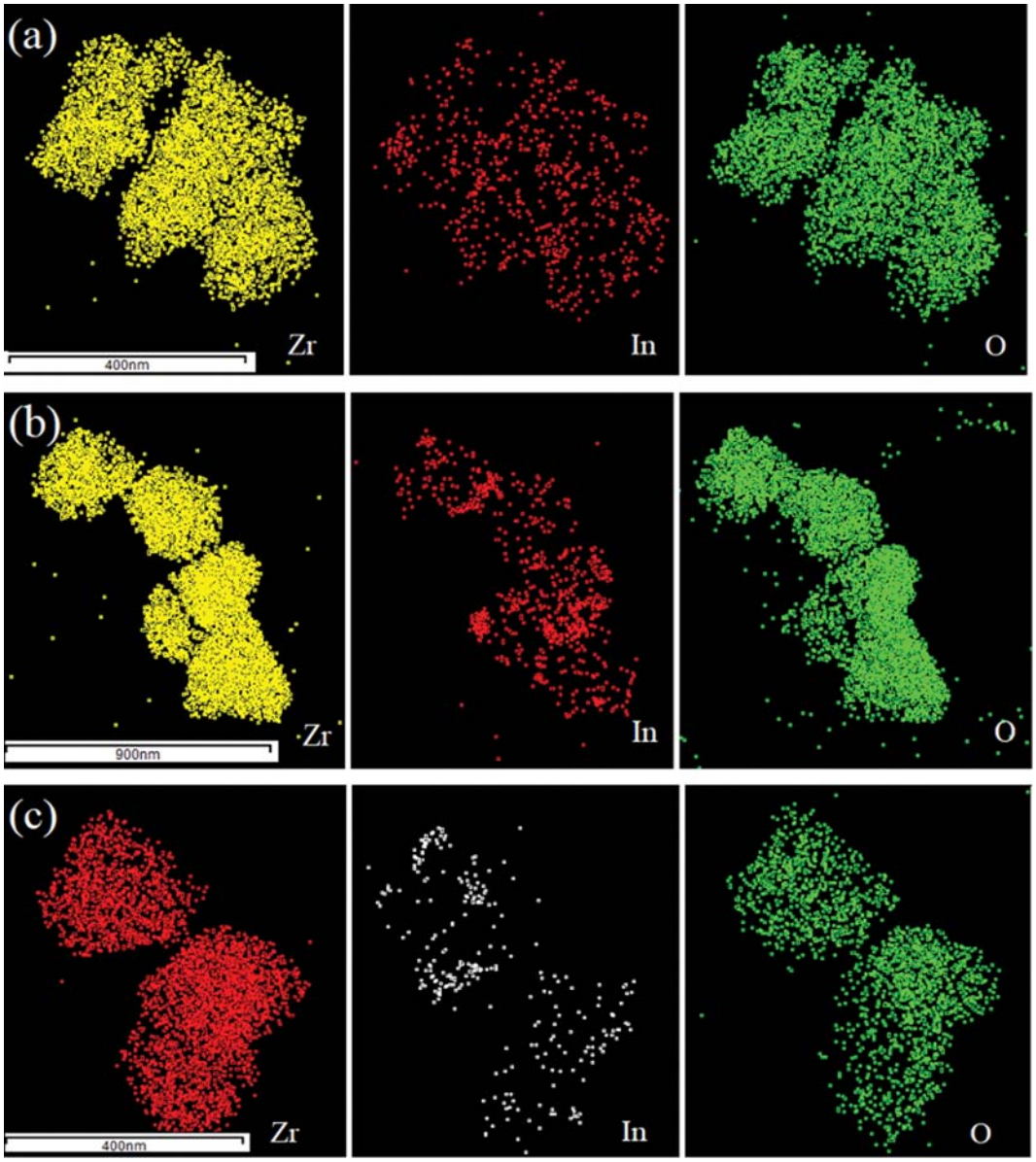

Fig. S4. TEM mapping showing elemental distribution of Zr, In and O on the surface of (a) In_2O_3/ZrO_2(SG), (b) In_2O_3/ZrO_2(UH) and (c) In_2O_3/ZrO_2(WI).

Table S1. Catalytic performance of the In_2O_3 catalysts in the CO_2 hydrogenation reaction

Catalyst	X_{CO_2} (%)	$S_{methanol}$ (%)	$Yield_{methanol}$ (%)	$STY_{methanol}$ ($g_{methanol}\ g_{cat}^{-1}h^{-1}$)	$Yield_{CO}$ (%)	STY_{CO} ($g_{CO}\ g_{cat}^{-1}h^{-1}$)
In_2O_3/ZrO_2(SG)	16.23	94.39	15.32	0.95	0.91	0.050
In_2O_3/ZrO_2(UH)	12.76	96.16	12.27	0.66	0.49	0.023
In_2O_3/ZrO_2(WI)	4.46	94.61	4.22	0.28	0.31	0.013
Bulk In_2O_3	6.99	95.56	6.68	0.44	0.23	0.018

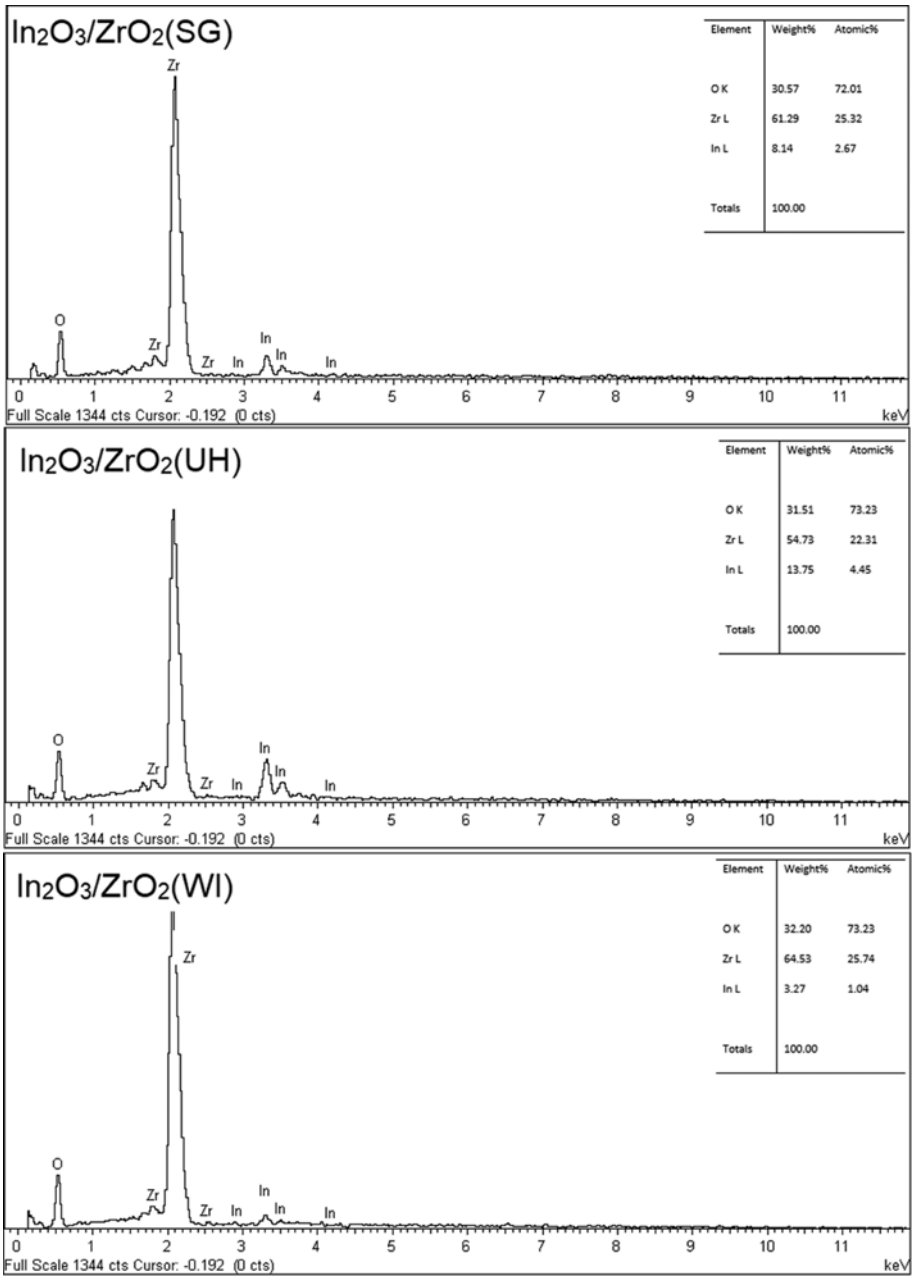

Fig. S5. EDX analysis of In_2O_3/ZrO_2 catalysts prepared by different synthesis routes.